IEEE Journal of
Microwaves

Performance Evaluation of Broadband Characterization of Coupled Transmission Lines Even- and Odd-Mode Propagation Constants Using Differential and Common Mode S-Parameters

MARIO PÉREZ-ESCRIBANO (Graduate Student Member, IEEE),
AND ENRIQUE MÁRQUEZ-SEGURA (Senior Member, IEEE)

(Regular Paper)

Telecommunication Research Institute (TELMA), E.T.S. Ingeniería de Telecomunicación, Universidad de Málaga, 29016 Málaga, Spain

CORRESPONDING AUTHOR: Enrique Márquez-Segura (e-mail: ems@ic.uma.es).

ABSTRACT This work encompasses some relevant issues that arise when using a broadband method to characterize the even and odd mode propagation constants of symmetric microstrip coupled lines using four-port pure-mode differential and common mode S-Parameters. Correct excitations of differential and common modes play a significant role in experimental results. From these 4-port measurements, parameters corresponding to the even and odd modes can be extracted from the multi-mode generalized S-parameters obtained by the vector network analyzer. Differential and common mode sub-matrices are considered as two independent equivalent 2-port transmission lines. The method will be applied to extract the propagation constants of even and odd modes of coupled microstrip transmission lines. A discussion is included on ensuring the correct excitation of the modes in the structure and avoiding possible unwanted effects such as radiation, that negatively affects the final estimation, both in phase and attenuation. Two figures of merit are defined to evaluate how transitions affect the performance of the method. These figures of merit allow a reasonable estimation of how the final experiment is affected by selected excitation of modes. To assess the theory presented, two sets of seven lines of different lengths are manufactured. The experimental results show an excellent agreement, both with electromagnetic simulations and with the analytical model used, for the phase constant in the improved case of 30° bends, and an improvement in the useful bandwidth of the attenuation constant. This fact verifies the correct functioning of the method. In addition, the measurements are presented in the range of 0.01–67 GHz, which represents a significant advance in bandwidth for this type of structure.

INDEX TERMS Broadband measurements, coupled microstrip lines electromagnetic (EM) characterization, propagation constant, transmission line measurements.

I. INTRODUCTION

Characterization techniques for symmetric coupled transmission lines have been a topic of active research for years since the use of differential circuits is notably increasing in microwave technology. This particular case of multiconductor transmission lines is widely used for several applications in the microwave and millimeter-wave frequency bands where devices such as filters [1], power dividers [2], and directional couplers [3] are extensively used. The knowledge of the actual propagation constant of quasi-TEM modes is of great
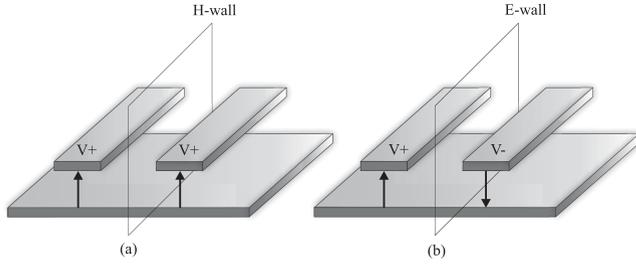
FIGURE 1. Field configuration of coupled lines even (a) and odd (b) modes.

relevance, especially for broadband applications, as well as the difference in phase velocities, and therefore, dispersion characteristics of modes propagating in the structure limit remarkably the operational bandwidth of the device as it is well-known [4].

In a pair of symmetric coupled transmission lines, as depicted in Fig. 1, the propagation mode is a combination of the odd and even modes [5]. A modal analysis for extraction of multimode propagation constants was presented in [6]. In general terms, several methodologies have been proposed in the literature to characterize the propagation constants of coupled transmission lines. On the one hand, resonant methods [7], [8] look to force resonances in the structure, and it is possible to obtain a fairly accurate value of the propagation constant. Their main drawback is that they only offer a solution in a limited number of frequencies, only at those frequencies where resonances occur. On the other hand, broadband methods [9], [10] allow estimating, ideally, a solution that covers the entire frequency sweep of the analyzer. Nevertheless, these works were limited to 20 GHz. For example, in [10] a method based on reflection measurements is considered to take advantage of a destructive setup considering the invariance of the cross-ratio of four complex numbers to a bilinear transformation. However, for all broadband methods, their main inconvenience is the lack of accuracy when estimating the attenuation constant of low-loss transmission media. In [11], a SPICE-compatible equivalent circuit model of on-chip coupled transmission lines was extracted, using a similar procedure to the one in [12]. Regarding asymmetric coupled transmission lines, in [13], it was presented a method to characterize asymmetric coupled lines when the modal cross powers are significant, based on relations between the transmission line's conductor representation, its modal representation, and its impedance matrix. The extraction of propagation constants is also the basis of the SPP light method used in [14].

The characterization of differential devices can be performed using a pure-mode four-port vector network analyzer. In this case, two generators are used to provide differential and common mode excitation to the device under test. It is well known that this characterization is necessary for active differential devices due to inherent nonlinearity. Meanwhile, a conventional four-port vector analyzer for passive devices is enough using the mixed-mode transformation [15], [16]. In

passive devices, conversion mode sub-matrices uncertainties are reduced using a pure-mode vector network analyzer [17]. From pure-mode S-parameters, in [18] it was proposed to characterize coupled microstrip lines from the transmission line approach model in [19]. Regarding calibration, in [20], a multimode through-line-reflect (TRL) calibration based on generalized reverse cascade matrices was presented. In [21], multimode TRL calibration was applied for the characterization of homogeneous differential discontinuities.

This paper deeply studies the effects of the excitation of even and odd modes for accurately modeling lossy coupled transmission lines over a very broad frequency band. The studied method pays special attention to the accurate characterization of the attenuation constant, known as a problematic parameter to be determined using broadband methods. For this purpose, long lines can be used to increase measured insertion losses, and the accuracy can be increased if higher differences in line lengths are used [22]. The procedure for measuring differential S-parameters, using a pure-mode network analyzer, as well as the separation of parameters of the even and odd modes, are explained in Section II. Section III shows the process of applying the method to each of the even and odd mode matrices to extract the real and imaginary parts of the propagation constant. Section IV discusses how the excitation of the modes of the coupled transmission lines influences the correct operation of the method. Section V includes the analytical, simulated, and measured results of the performed experiment to validate the presented theory. Conclusions are given in Section VI.

II. S-PARAMETERS OF SYMMETRIC COUPLED LINES

In a pair of microstrip coupled transmission lines two independent quasi-TEM modes propagate: the even and odd modes, as mentioned above. A diagram of the field configuration of these modes is shown in Fig. 1. Their characteristic impedances, Z_{0_o} and Z_{0_e}, can be calculated analytically from the line parameters following the Kirschning and Jansen model [23]. From these characteristic impedances, and considering that the DUT is symmetric and reciprocal, the S-parameters of each mode of the transmission line can be computed as

$$S_{11_o} = S_{22_o} = \frac{\left(Z_{0_o}^2 - Z_0^2\right)\sinh\left(\gamma_o l\right)}{2Z_0 Z_{0_o}\cosh\left(\gamma_o l\right) + \left(Z_{0_o}^2 + Z_0^2\right)\sinh\left(\gamma_o l\right)},$$

$$S_{12_o} = S_{21_o} = \frac{2Z_0 Z_{0_o}}{2Z_0 Z_{0_o}\cosh\left(\gamma_o l\right) + \left(Z_{0_o}^2 + Z_0^2\right)\sinh\left(\gamma_o l\right)},$$

$$S_{11_e} = S_{22_e} = \frac{\left(Z_{0_e}^2 - Z_0^2\right)\sinh\left(\gamma_e l\right)}{2Z_0 Z_{0_e}\cosh\left(\gamma_e l\right) + \left(Z_{0_e}^2 + Z_0^2\right)\sinh\left(\gamma_e l\right)},$$

$$S_{12_e} = S_{21_e} = \frac{2Z_0 Z_{0_e}}{2Z_0 Z_{0_e}\cosh\left(\gamma_e l\right) + \left(Z_{0_e}^2 + Z_0^2\right)\sinh\left(\gamma_e l\right)},$$

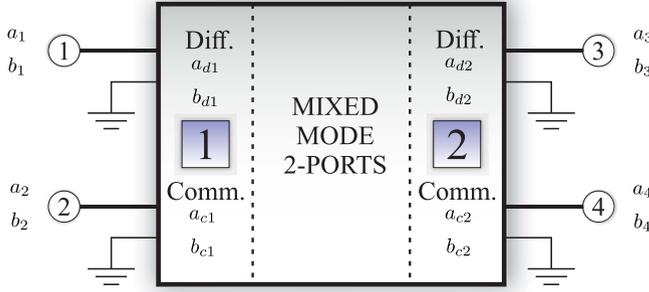$$(1)$$

IEEE Journal of Microwaves

FIGURE 2. Diagram of the mixed-mode S-parameters measurement. Circled numbers 1 to 4 represent single mode conventional ports. quared numbers 1 and 2 represent the mixed mode ports.

being γ_e and γ_o the propagation constant of even and odd modes respectively, and Z_0 the impedance of each external port. However, these S-parameters can not be measured independently. Instead, what is measured is a combination of both since they propagate simultaneously unless a pure-mode excitation is established.

A. DIFFERENTIAL S-PARAMETERS

To measure the S-parameters of each mode, from which its propagation constant is going to be estimated, mixed-mode S-parameters can be used. D. Bockelman and W. Eisenstadt introduced them in 1995 [24] to model differential circuits and devices using single-ended S-Parameters. Considering these parameters, it is possible to characterize more precisely the behavior of the common and differential modes of this type of devices independently [17]. Conversion starts from a single-ended measurement of a four-port device ($[S_{se}]$), which is transformed into an equivalent device with two ports that include both the differential and common modes ($[S_{mm}]$). Fig. 2 shows a diagram of the operation of mixed-mode S-parameter measurement, where the four single-ended ports are considered as two ports, propagating differential and common modes independently.

The single-ended S-parameters are given by

$$\begin{pmatrix} b_1 \\ b_2 \\ b_3 \\ b_4 \end{pmatrix} = \underbrace{\begin{pmatrix} S_{11} & S_{12} & S_{13} & S_{14} \\ S_{21} & S_{22} & S_{23} & S_{24} \\ S_{31} & S_{32} & S_{33} & S_{34} \\ S_{41} & S_{42} & S_{43} & S_{44} \end{pmatrix}}_{[S_{se}]} \cdot \begin{pmatrix} a_1 \\ a_2 \\ a_3 \\ a_4 \end{pmatrix}, \quad (2)$$

whereas the mixed-mode ones are given by

$$\begin{pmatrix} b_{d_1} \\ b_{d_2} \\ \hline b_{c_1} \\ b_{c_2} \end{pmatrix} = \underbrace{\begin{pmatrix} S_{dd_{11}} & S_{dd_{12}} & S_{dc_{11}} & S_{dc_{12}} \\ S_{dd_{21}} & S_{dd_{22}} & S_{dc_{21}} & S_{dc_{22}} \\ \hline S_{cd_{11}} & S_{cd_{22}} & S_{cc_{11}} & S_{cc_{12}} \\ S_{cd_{21}} & S_{cd_{22}} & S_{cc_{21}} & S_{cc_{22}} \end{pmatrix}}_{[S_{mm}]} \cdot \begin{pmatrix} a_{d_1} \\ a_{d_2} \\ \hline a_{c_1} \\ a_{c_2} \end{pmatrix}. \quad (3)$$

The matrix in (3) can be viewed as four sub-matrices corresponding to pure differential mode (S_{dd}), pure common

mode (S_{cc}), and the sub-matrices S_{dc} and S_{cd}, representing the transfer of energy between the differential and common modes. S_{dc} and S_{cd} are usually named cross-mode matrices. Matrices (2) and (3) can be related using [24]

$$[S_{mm}] = [M][S_{se}][M]^{-1}, \quad (4)$$

being

$$[M] = \frac{1}{\sqrt{2}} \begin{pmatrix} 1 & -1 & 0 & 0 \\ 0 & 0 & 1 & -1 \\ 1 & 1 & 0 & 0 \\ 0 & 0 & 1 & 1 \end{pmatrix}. \quad (5)$$

In a way, symmetric coupled lines work as differential devices, in which the odd mode corresponds to a differential excitation, whereas the even mode to a common one, as depicted in Fig. 1. However, this assumption would only be entirely true if both modes had a reference impedance of 50 Ω. Taking into account the different impedances of the even and odd modes, the transformation to be performed is

$$[S_{mm}] = ([M_1][S_{se}] + [M_2]) ([M_1] + [M_2][S_{se}])^{-1}, \quad (6)$$

where $[M_1]$ and $[M_2]$ can be calculated following the procedure described in [25]. If the lines were uncoupled, the condition $Z_0 = Z_{0_o} = Z_{0_e}$ would be fulfilled and $[M_2] = [0]$, $[M_1] = [M]$, and therefore, (6) reduces to (4).

The cross-mode parameters can be assumed as negligible in correctly excited coupled microstrip lines, so $S_{cd_{ij}} = S_{dc_{ij}} = 0 \forall i, j$, and the sub-matrices can be decoupled as

$$\begin{pmatrix} b_{d_1} \\ b_{d_2} \end{pmatrix} = \begin{pmatrix} S_{dd_{11}} & S_{dd_{12}} \\ S_{dd_{21}} & S_{dd_{22}} \end{pmatrix} \cdot \begin{pmatrix} a_{d_1} \\ a_{d_2} \end{pmatrix}, \quad (7a)$$

$$\begin{pmatrix} b_{c_1} \\ b_{c_2} \end{pmatrix} = \begin{pmatrix} S_{cc_{11}} & S_{cc_{12}} \\ S_{cc_{21}} & S_{cc_{22}} \end{pmatrix} \cdot \begin{pmatrix} a_{c_1} \\ a_{c_2} \end{pmatrix}. \quad (7b)$$

These parameters will be the starting point of the considered method for the estimation of the propagation constant: (7a) will be used for the odd mode and (7b) for the even one. Nowadays, depending on their configuration, network analyzers allow measuring differential and common mode S-parameters directly, without performing any transformation, provided they have the option to perform pure-mode measurements using two different tone generators [26]. In this work, we use a VNA which includes two independent tone generators so pure mode differential and common mode generation on every subset of two ports are available.

B. PURE-MODE NETWORK ANALYZERS

Pure-mode measurements were introduced in [27]. To perform them, it is necessary the availability of a pure-mode vector-network analyzer (PMVNA). For this type of measurement, four physical ports must be used. The main idea is to generate the four virtual ports shown in Fig. 2 associating 2 for the common mode and 2 for the differential mode. For this purpose, it must be ensured that there is a phase difference of 0° and 180° between physical ports 1 and 2,
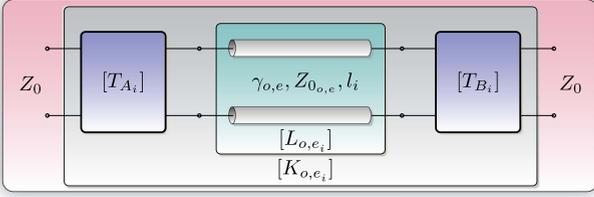
This article has been accepted for inclusion in a future issue of this journal. Content is final as presented, with the exception of pagination.

PÉREZ-ESCRIBANO AND MÁRQUEZ-SEGURA: PERFORMANCE EVALUATION OF BROADBAND CHARACTERIZATION

FIGURE 3. Concatenation diagram of the transmission line T-parameters for simulation and measurement.

and ports 3 and 4, respectively, to generate real common and differential excitations. From these excitations, it is possible to obtain, directly from the network analyzer, the mixed-mode S-parameters matrix ($[S_{mm}]$). It is essential to highlight the need for the network analyzer to have two different tone generators operating simultaneously. It was demonstrated that PMVNA uncertainty is lower for cross-mode parameters than that of a traditional four-port vector network analyzer when measuring differential devices [17].

III. DESCRIPTION OF METHOD BASED ON TRANSMISSION LINES OF DIFFERENT LENGTHS

The method used estimates the propagation constant of 2-port transmission lines in broadband. It is based on the one proposed by Bianco and Parodi in [28] and later used in TRL calibration [29], [30] to get the propagation constant value. The key to using it for coupled lines is to work independently with odd and even mode matrices, previously separated, measured using a PMVNA. It is relevant to convey that the characteristic impedance cannot be estimated using this kind of method based on two-port mathematical invariants. Any transmission line of a given impedance Z_{0_x} can be transformed into another transmission line of impedance Z_{0_y} with ideal transformers in cascade, whose turns ratio depends on both impedances values [31]. This ideal transformer is therefore embedded in the transitions considered as linear two-port circuits ($[T_{A_i}]$, $[T_{B_i}]$), and information is lost as matrices invariants are the core of the method used. The characteristic impedance can be calculated afterward using the propagation constant estimated using several strategies [32] or even time domain techniques if available afterward. Similar behavior is noticeable in coupled transmission lines [33]. The procedure starts with the measurement of the S-parameters of two coupled lines of different lengths. To concatenate parameters, a transformation to T-parameters is performed. As seen in Fig. 3, these parameters ($[K_{o,e}]$) include both the effects of the transitions ($[T]$) and those of the transmission line ($[L_{o,e}]$). In this way, $[K_i]$, which will be different for each propagation mode, can be expressed as $[K_{o,e_i}] = [T_{A_i}][L_{o,e_i}][T_{B_i}]$ ($i = \{1, 2\}$, $i = 1$ represents the shortest line, and $i = 2$, the longest one). However, this expression includes both the effects of transitions and the effect of the line. To solve this problem, a mathematical transformation must be applied to eliminate the effect of transitions. This is done by measuring

lines of different lengths and using the mathematical concept of invariants [34]. This process assumes that matrices $[T_{A_i}]$ and $[T_{B_i}]$ are invariants for every line, so from now on, they will be considered as $[T_A]$ and $[T_B]$. Since this concept was raised, there have been several mathematical strategies to isolate the effect of the line from that of the transitions. On the one hand, there are strategies based on the calculation of traces or determinants of matrices. However, in [35] it was shown that the most efficient strategy was to use methods based on eigenvalues since these are the least affected by random errors. For this reason, an eigenvalue-based variant method will be used in this paper. The starting point is T-parameters matrices $[K_{o,e_1}]$ and $[K_{o,e_2}]$. These matrices can be combined following

$$[K_{o,e_1}][K_{o,e_2}]^{-1} = [T_A][L_{o,e_1}][L_{o,e_2}]^{-1}[T_A]^{-1}. \quad (8)$$

This equation can be rewritten if matrices $[K_{o,e}]$ and $[L_{o,e}]$ are defined as $[K_{o,e}] = [K_{o,e_1}][K_{o,e_2}]^{-1}$ and $[L_{o,e_1}][L_{o,e_2}]^{-1}$, so (8) can be expressed as

$$[K_o] = [T_A][L_o][T_A]^{-1},$$
$$[K_e] = [T_A][L_e][T_A]^{-1}. \quad (9)$$

Equation (9) is a similarity transformation, so $[K_{o,e}]$ and $[L_{o,e}]$ are similar matrices and, therefore, their eigenvalues, determinants, and traces coincide. Being $\gamma_o = \alpha_o + j\beta_o$, $\gamma_e = \alpha_e + j\beta_e$, $\Delta l = l_2 - l_1$, and matrices $[L_o]$, $[L_e]$ are diagonal matrices defined as

$$[L_o] = \begin{bmatrix} e^{+\gamma_o \Delta l} & 0 \\ 0 & e^{-\gamma_o \Delta l} \end{bmatrix},$$
$$[L_e] = \begin{bmatrix} e^{+\gamma_e \Delta l} & 0 \\ 0 & e^{-\gamma_o \Delta l} \end{bmatrix}, \quad (10)$$

and its eigenvalues are $\lambda_1 = e^{-\gamma_{o,e}\Delta l}$ and $\lambda_2 = e^{+\gamma_{o,e}\Delta l}$. These eigenvalues coincide with those of matrix $[K_{o,e}]$. In this way, the de-embedding process is performed by the method itself. Therefore, the propagation constants γ_o and γ_e can be calculated using

$$\gamma_o = \frac{1}{\Delta l} \ln\left(\frac{1/\lambda_{1_o} + \lambda_{2_o}}{2}\right),$$
$$\gamma_e = \frac{1}{\Delta l} \ln\left(\frac{1/\lambda_{1_e} + \lambda_{2_e}}{2}\right) \quad (11)$$

respectively. At this point, it is important to mention that if the obtained method were applied to two-port single transmission lines, it would not be required to calibrate the analyzer since the effects of transitions have been eliminated by introducing the concept of invariant. A deeper discussion can be found in [35]. In the case of using a pure-mode vector network analyzer to use ports combined to establish common and differential excitation, a SOLT calibration must be performed to establish the phase reference for 0° and 180°.

Although this way of obtaining the propagation constant would be sufficient under ideal conditions, the truth is that the presence of random errors due to manufacturing or the
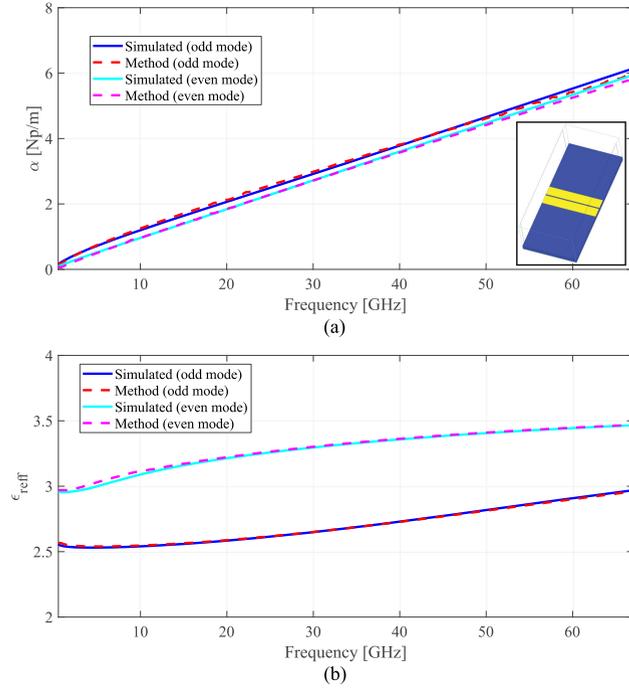
FIGURE 4. Attenuation constant (a) and effective relative permittivity (b) obtained from port simulations and considering S-parameters matrices using the proposed method.

FIGURE 5. Configuration of coupled lines using no bend (ideal case) (a), 90° (b), and 30° (c) bends. Note that (a) is only possible in analytical or simulation scenarios.

measurement system reduces the method's accuracy. That is why many authors have proposed increasing the number of lines to obtain a more precise broadband characterization. In [35], it was shown that the standard deviation of random errors decreases as the number of lines increases. To improve the accuracy of the method, it is proposed to use a least-squares fit, which is the maximum likelihood estimator for a Gaussian distribution of random errors, solving the equation in a similar way as single mode but independently for every mode, differential, and common modes,

$$\min_{\alpha_o,\beta_o} \frac{1}{2} \sum_{n=1}^{N} \left| \left(\frac{1/\lambda_{1_{no}} + \lambda_{2_{no}}}{2} \right) - e^{+(\alpha_o + j\beta_o)\Delta l} \right|^2,$$

$$\min_{\alpha_e,\beta_e} \frac{1}{2} \sum_{n=1}^{N} \left| \left(\frac{1/\lambda_{1_{ne}} + \lambda_{2_{ne}}}{2} \right) - e^{+(\alpha_e + j\beta_e)\Delta l} \right|^2 \quad (12)$$

where N is the number of possible combinations between all the i lines, and λ_{1_n}, λ_{2_n} the eigenvalues corresponding to combination n. The lengths of these lines can be chosen considering a quasi-linear or logarithmic criterion, as explained in [35].

Regarding mixed-mode S-parameters measurement, the transformation carried out in (4) does not change the method behavior, since, like (9), both equations are similarity transformations. To validate the operation of the proposed method in an ideal case, two pairs of coupled lines, like the ones in Fig. 1, have been simulated in the full-wave simulator AN-SYS HFSS [36]. This simulation corresponds to the structure
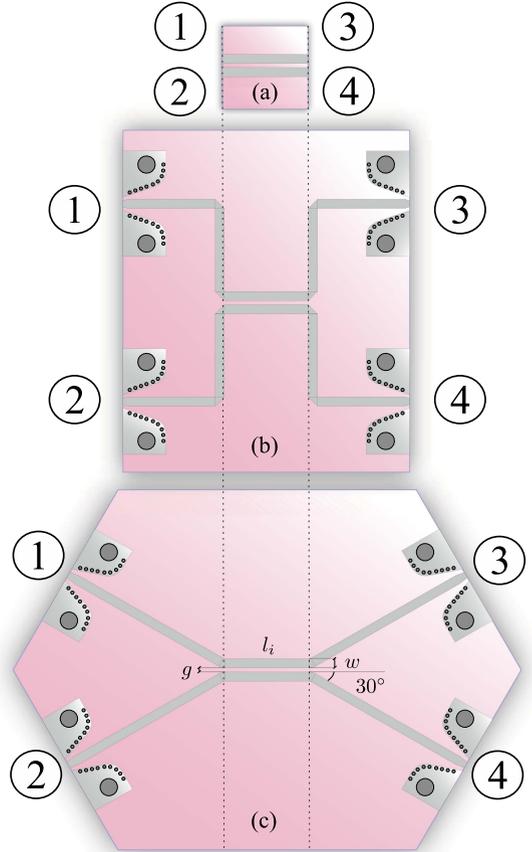
depicted in Fig 5(a). Using these simulations, comparison by mixed-mode or single-mode ports is possible. In real system transitions, bends and connectors must be used. For this purpose, it has been used Rogers 4350B substrate, with 508 μm thickness, $\varepsilon_r = 3.66$, $\tan \delta = 0.0031$, and 17.5 μm thick copper metallization. The relative permittivity of the substrate up to 50 GHz has been imported using the dispersion model provided in [37]. The line widths are set to 1.095 mm, to get a 50 Ω characteristic impedance at interface ports, whereas the lengths are 10 and 35 mm, respectively. The gap between lines is set to 150 μm.

As mentioned above, two types of simulations have been carried out. On the one hand, a modal simulation has been used, from which the constant propagation of even and odd modes in the ports of the structure is obtained, ($[S_{mm}]$). On the other hand, a terminal simulation has been carried out in which the 4-port S-parameter matrix of the structure ($[S_{se}]$) is obtained. The transformation to differential S-parameters is applied to this matrix, obtaining the matrices of the even and odd modes to which the considered method is applied, no matter whether pure mode or conversion is used. Fig. 4 shows the results using both simulations, as well as an inset picture of the simulated structure. For ease of view, the
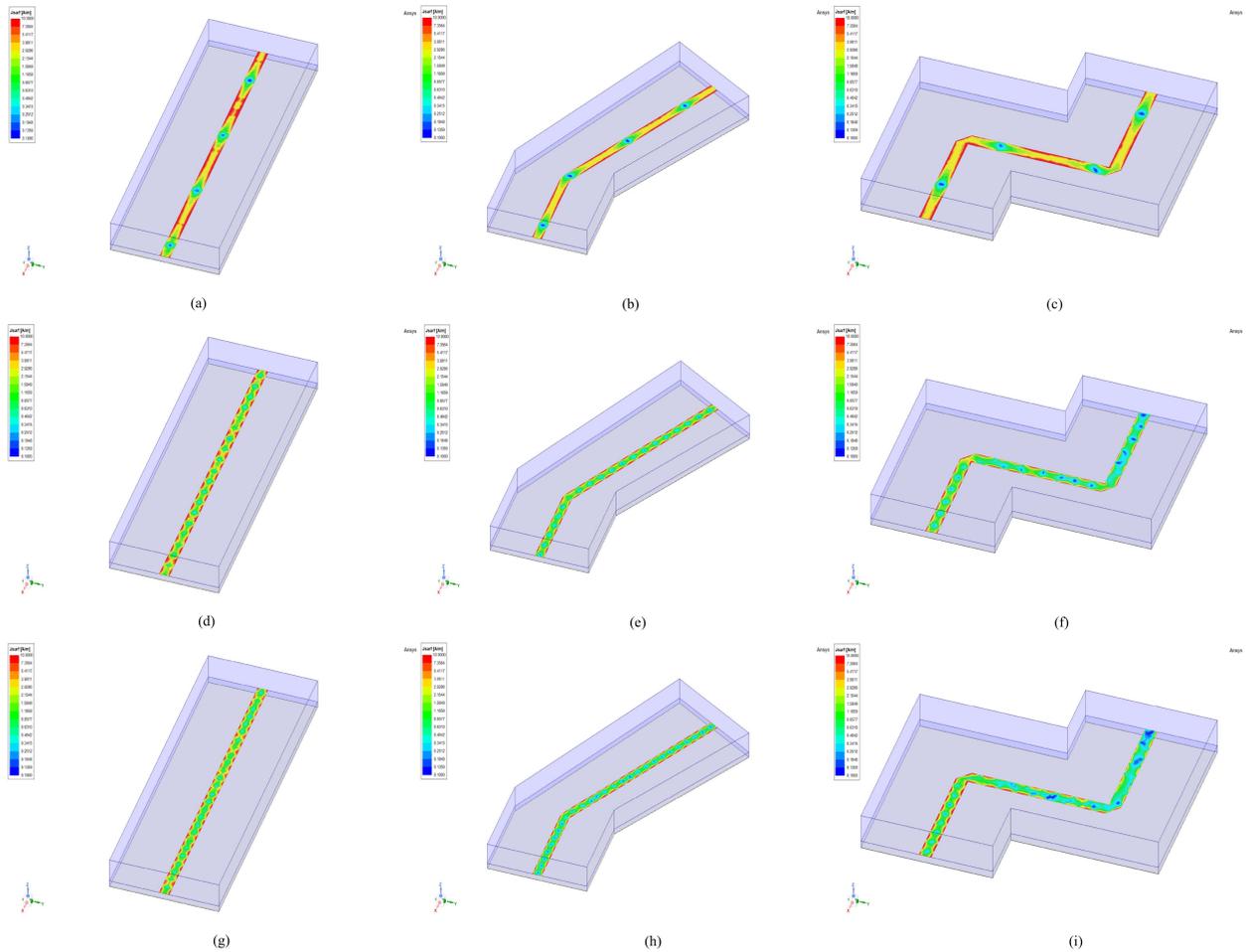
This article has been accepted for inclusion in a future issue of this journal. Content is final as presented, with the exception of pagination.

PÉREZ-ESCRIBANO AND MÁRQUEZ-SEGURA: PERFORMANCE EVALUATION OF BROADBAND CHARACTERIZATION

FIGURE 6. Current density, *J*, at 10 GHz (a), (b), (c), 50 GHz (d), (e), (f) and 67 GHz (g), (h), (i) using an ideal feeding line, and 30° and 90° bends.

phase constant is represented in terms of effective relative permittivity, using the transformation $\varepsilon_{r,eff_{o,e}} = (c\beta_{o,e}/\omega)^2$. As seen, both the simulated propagation constants and the ones obtained from the proposed method clearly coincide. The results show the method's validity to obtain the propagation constant of both modes in simulation for a structure like the one in Fig. 5(a). Thus, it is shown that the theory explained in Section II for single-ended measurements, transforming them to differential and common mode matrices using (4) (as simulations are performed) is valid to obtain the S-parameters of the even and odd modes correctly. Modal simulation results are equivalent to the pure-mode measurements that were mentioned above.

The problem arises when trying to validate the method experimentally. It is necessary to place connectors at the end of the lines. These connectors do not fit in the configuration of two coupled lines, so it will be necessary to look for a configuration based on bends that makes it possible to feed the lines separating the access ports. A deeper discussion will be presented in the next section discussing how a proper selection of feeding transmission lines is necessary to get the best possible results.

IV. MODES EXCITATION

To place the connectors at the edges, it is necessary to get enough space, so they fit in the structure. For that reason, bends are used to adequately separate connectors. First, a simple structure with two 90° mitered bends for each port is proposed, as shown in Fig. 5(b). As all the access lines are the same, it is guaranteed that coupled lines will have a differential or common mode correct excitation. However, for PMVNA measurements, it is necessary to use a SOLT calibration that compensates for the differences between the analyzer ports to ensure that ports can have differential or common mode excitations. It is noteworthy that this is a substantial difference compared to when the studied method is applied for single-mode 2-port transmission lines.

The main problem associated with bends in literature is radiation losses [38]. These losses are especially significant when the angle of the bends increases [39] and at high frequencies when the length of lines between bends is comparable with guided wavelength. For this reason, an additional configuration with only a 30° bend is considered and depicted in Fig. 5(c). The use of 30° bends still allows a proper connection to the VNA. Lower values can be used, but 30° is
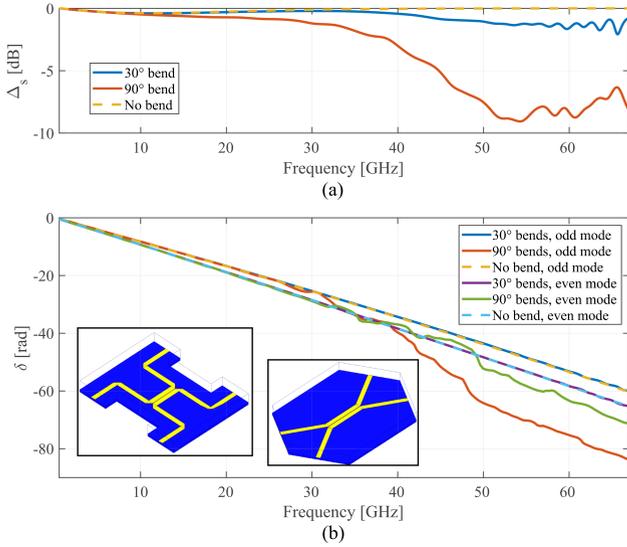
FIGURE 7. Δ (a) and δ (b) figures of merit using 90°, 30°, and no bends and lines of 10 and 35 mm.

a balance between admissible parasitic effects and adequate connections with reasonable lengths for feeding microstrip lines. To show the degradation suffered by the signal as it passes through the bends, the current density, J, at 10, 50, and 67 GHz, has been plotted in Fig. 6, for a straight ideal transmission line (Fig. 5(a)) and the two proposed bends configuration (Fig. 5(b) and (c)). As seen, at 10 GHz, the behavior is quite similar, but when increasing frequency, the current density distribution degrades considerably after propagating through the bends. However, the 30° configuration shows a behavior much more similar to that of the ideal line than the 90° one.

To show the effect of the bends, two figures of merit are proposed to compare how the two configurations can affect the considered method, which are key to understanding how the method works. This way, an evaluation of the subsequent results can be done before fabrication to ensure useful results. On the one hand, the attenuation constant strongly depends on the absolute value of the S-parameters [35]. To satisfy energy conservation, the equation

$$\sum_{n=1}^{N} |S_{nm}|^2 \leq 1 \; \forall m \tag{13}$$

must be fulfilled for each line [40]. In this sense, and to evaluate radiation losses, the energy conservation expression can be used as a figure of merit Δ_s and can be defined, for the feeding lines (see Fig. 6), as

$$\Delta_s = |S_{11}|^2 + |S_{21}|^2 \leq 1. \tag{14}$$

Referring to the 4-port structure, the equivalent figure of merit, using the common and differential mode S-parameters, can be written as follows

$$\Delta_o = |S_{dd_{11}}|^2 + |S_{dd_{21}}|^2 + |S_{dc_{11}}|^2 + |S_{dc_{21}}|^2 \leq 1, \tag{15a}$$
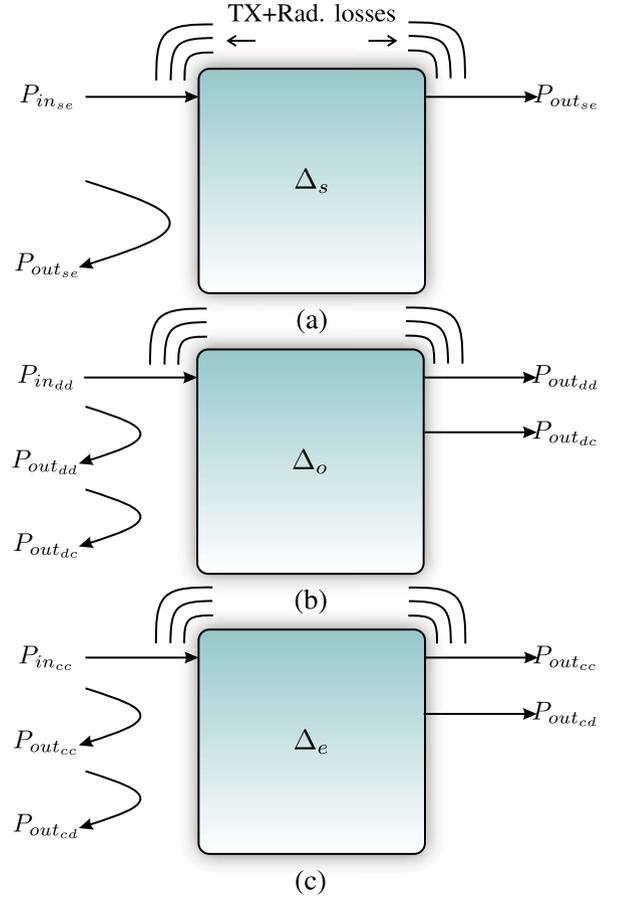

FIGURE 8. Power scheme for the definitions of Δ parameters. (a) Single-mode straight transmission line. (b) Differential/odd mode excitation. (c) Common/even mode excitation.

$$\Delta_e = |S_{cc_{11}}|^2 + |S_{cc_{21}}|^2 + |S_{cd_{11}}|^2 + |S_{cd_{21}}|^2 \leq 1. \tag{15b}$$

These figures include the transmitted and reflected power in the same mode and between differential and common ones. The relationship between the input and output power is represented in the diagram of Fig. 8 for the three different Δ parameters defined.

On the other hand, the phase constant depends on the phase difference between two lines with different lengths. For this reason, appropriate figures of merit δ_o and δ_e can be defined as

$$\delta_o = \angle S_{dd_{21_2}} - \angle S_{dd_{21_1}} \tag{16a}$$

$$\delta_e = \angle S_{cc_{21_2}} - \angle S_{cc_{21_1}}. \tag{16b}$$

If the lines were well matched, the phase difference between two lines of different lengths would be completely linear. If there is no matching, as happens when bends are introduced, the phase difference will not be linear, but its trend will still be linear. This fact can be effortlessly checked when evaluating (1) for two lines with $Z_{o,e} \neq Z_0$.

The two defined figures of merit will serve to evaluate how bends can affect the behavior of the considered method. On

the one hand, Fig. 7(a) shows the simulated Δ_s for an ideal feeding line and the two proposed configurations based on bends. It is a lossless simulation, in order to isolate the effects of the radiation. As can be seen, there is much greater power loss due to radiation when using 90° bends, finding a similar behavior to the straight line (no bend case) when using the 30° configuration. This irregular behavior will cause the estimated attenuation constant to deteriorate rapidly. Bad results are expected for α even at low frequencies beyond 20 GHz (Fig. 7(a)).

On the other hand, δ is plotted in Fig. 7(b) for the two lines simulated in the previous section using 30° and 90° bends, and for the ideal case that has no bends. For the 90° bends configuration, the phase difference does not have a linear behavior with frequency, which is a fundamental condition for the correct functioning of the method [35]. For this reason, the phase constant will not be correctly calculated at high frequency, as will be seen in the experimental validation. Therefore, 30° bends configuration is expected to make the method works better, as the phase difference, δ, is almost the same as the ideal case, as depicted in Fig. 7(b).

In the microstrip prototype fabricated, no propagation of TM_0 surface wave mode has been verified by simulation. Another problem that could affect the performance of the method is the propagation of higher-order modes, which limits the useful bandwidth of the microstrip [41], [42]. However, the first mode of interest, which corresponds to a Transverse Microstrip Resonance, does not propagate up to 60.8 GHz for the microstrip dimensions and substrate used, so it is ruled out that the propagation of higher-order modes could limit the performance of the considered method. The slab-mode, and high-order microstrip modes, including microstrip surface wave modes, do not propagate even out of the bandwidth of the used vector network analyzer.

V. ASSESSMENT OF THE METHODOLOGY

To assess the performance of the considered method, several experiments have been carried out. Two of them are presented to demonstrate experimentally the effect of different bend angles using RO4350B substrates. Experiments consisted of 7 lines, whose lengths were chosen taking the quasi-linear (q = 1.2) criteria [35] (10, 12.91, 16.69, 20.88, 25.37, 30.09, and 35 mm). The first experiment has been manufactured using a substrate of 762 μm high and a line width of 1.65 mm and a gap of 200 μm. The second experiment uses a 508 μm high substrate, and the line width was set to 1.095 mm, with a gap between lines of 500 μm. On the one hand, the 90° experiment layout is as depicted in Fig. 5(c). On the other hand, the structure with 30° bends was used, like the one shown in Fig. 5(c). These structures were manufactured and subsequently measured using the network analyzer Agilent PNA-X (N5247 A). The VNA configuration was set up as follows: $f_{start} = 10$ MHz, $f_{stop} = 67$ GHz, and 6401 data points were taken, using a delay before measuring each point of 250 μs. The bandwidth of the IF bandpass filter was set at 10 kHz, whereas the port power to −5 dBm. The calibration kit for SOLT calibration

FIGURE 9. Photograph of manufactured coupled lines and the measurement setup using vector network analyzer for Pure Mode S-parameters measurement.

at external ports was the Agilent 85058E-1.85 mm. Results, as well as measured and simulated Δ and δ figures of merit, are depicted in Figs. 10 and 11. The analytical model used to compare with simulated and measured results is the one proposed by Hammerstad and Jensen in [43]. Simulated results have been obtained using a modal simulation of the ideal structure, without bends, in the full-wave simulator ANSYS HFSS. A photograph of the simulated structures is included in that figure. The measurement setup is depicted in Fig. 9.

Fig. 10 shows the experimental results for a 90° bend as transition for coupled lines excitation. The graph for the figure of merit Δ, Fig. 10(d), considered shows a great ripple that clearly affects the attenuation constant from very low frequencies. In the case of the effective permittivity, it is usable under 30 GHz but clearly not for upper frequencies. Useless results are shaded gray. Fig. 11 shows the experimental results for a 30° bend as transition for coupled lines excitation. As seen, the accuracy of the obtained attenuation constant is good up to 50 GHz. Regarding the effective relative permittivity, the results obtained are highly accurate, similar to those of the analytical and simulated models. Excellent results for the phase constant have been obtained in the full measured bandwidth, as the phase difference tendency remains linear (δ). Using 30° bends allows a significantly better performance of the method considered as predicted by the proposed figures of merit. Results are coherent with the use of the figure of merit proposed whose result can be compared by using Figs. 10(d) and 11(d) (Note different scales for clarity in both graphs). The attenuation constant is better than the one that could have been obtained using 90° bends, as Δ and δ are quite similar to the ones of the ideal feeding lines.
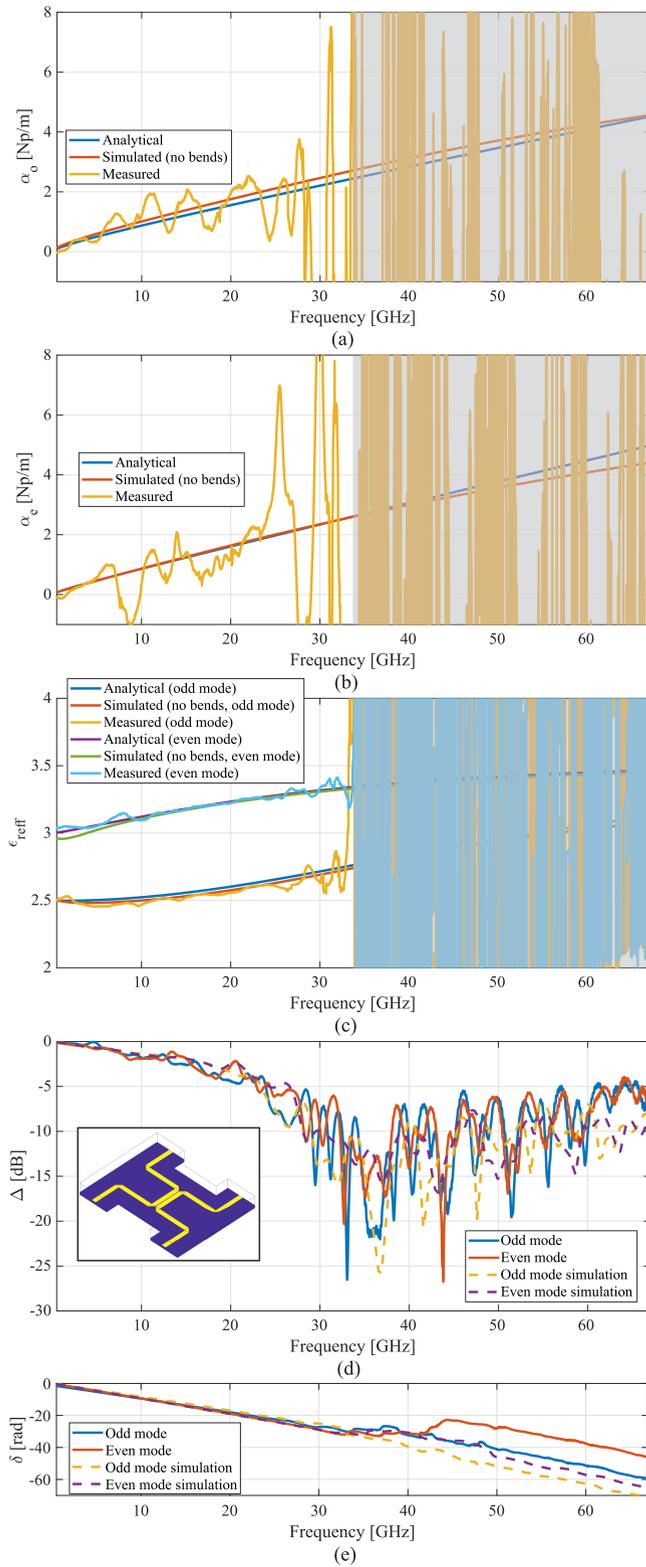
FIGURE 10. Experimental results of the attenuation constants and effective relative permittivities using the proposed methods with 90° bends (Fig. 5(b)), in comparison with electromagnetic simulation and analytical model, as well as simulated and measured Δ and δ figures of merit, using lines #1 and #7 (h = 762 μm, w = 1.65 mm, s = 200 μm).
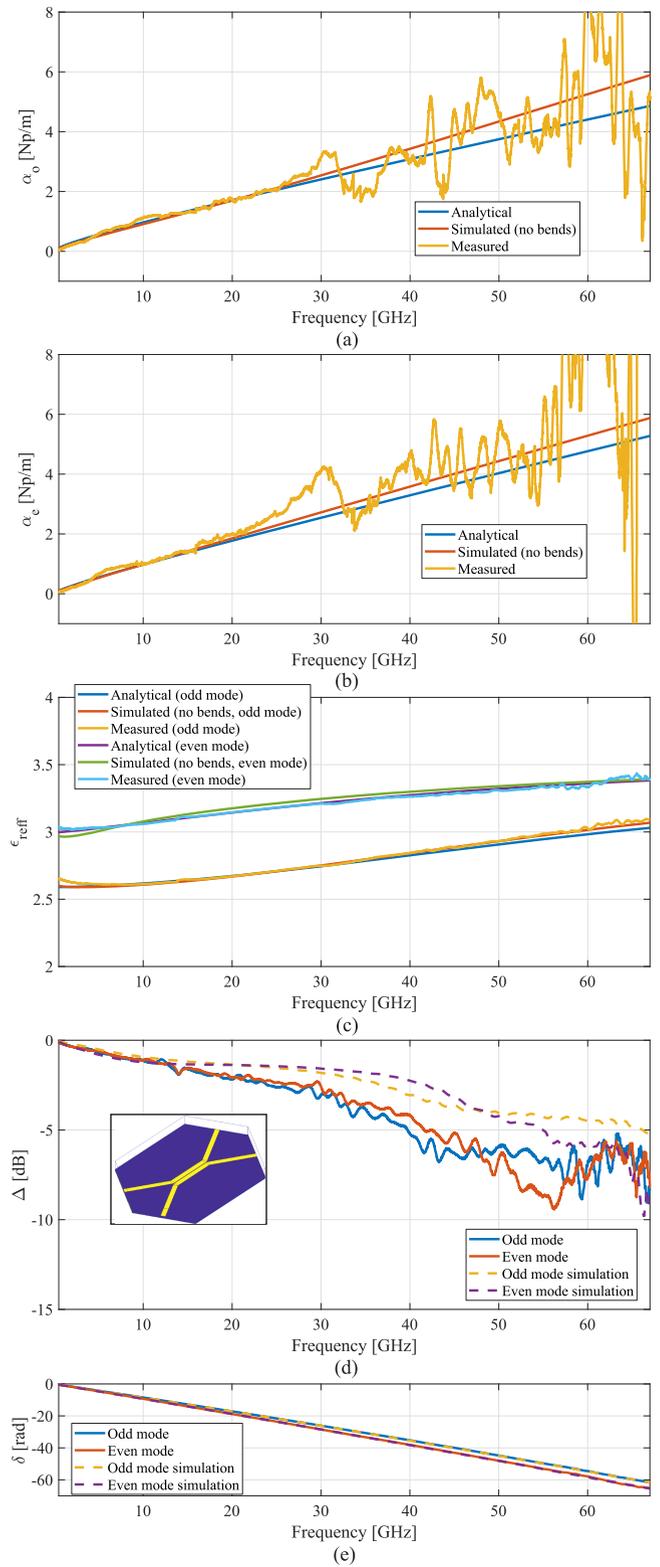

FIGURE 11. Experimental results of the attenuation constants and effective relative permittivities using the proposed methods with 30° bends (Fig. 5(c)), in comparison with electromagnetic simulation and analytical model, as well as simulated and measured Δ and δ figures of merit, using lines #1 and #7 (h = 508 μm, w = 1.095 mm, s = 500 μm).

VI. CONCLUSION

This work presents a study of the effects of the excitations when obtaining the even and odd modes propagation constant of microstrip coupled lines from 4-port pure-mode S-parameters measurements. The method uses the measures of different length coupled lines. It allows obtaining excellent results, in comparison with the analytical and simulated models, for the phase constant, whereas reasonable results are obtained for the attenuation constants over the entire measurement bandwidth (0.01–67 GHz), depending on the excitation of propagation modes involves. In this sense, a study has been performed, showing that reducing the angle of the bends improves the excitation of the modes, since radiation is drastically reduced, causing the result of the attenuation constant to be considerably enhanced and the bandwidth of the phase constant extended to the whole available frequency band. Two figures of merit have been defined to evaluate how the accuracy of the results can be improved. The experimental validation has served to assess the theory presented, showing very accurate results for the phase constant throughout the entire bandwidth of the vector network analyzer used. Therefore, it can be concluded that, despite its simplicity, the considered method using different-length transmission lines allows obtaining the propagation constant quite accurately as the bend angle is correctly chosen for mode excitation.

REFERENCES

[1] J. J. Sánchez-Martinez, E. Márquez-Segura, and S. Lucyszyn, "Synthesis and design of high-selectivity wideband quasi-elliptic bandpass filters using multiconductor transmission lines," *IEEE Trans. Microw. Theory Techn.*, vol. 63, no. 1, pp. 198–208, Jan. 2015.

[2] S. Kim, S. Jeon, and J. Jeong, "Compact two-way and four-way power dividers using multi-conductor coupled lines," *IEEE Microw. Wireless Compon. Lett.*, vol. 21, no. 3, pp. 130–132, Mar. 2011.

[3] A. R. Djordjević, V. Napijalo, D. I. Olćan, and A. Zajic, "Wideband multilayer directional coupler with tight coupling and high directivity," *Microw. Opt. Technol. Lett.*, vol. 54, pp. 2261–2267, 2012.

[4] B. Sheleg and B. Spielman, "Broad-band directional couplers using microstrip with dielectric overlays," *IEEE Trans. Microw. Theory Techn.*, vol. 22, no. 12, pp. 1216–1220, Dec. 1974.

[5] R. S. Elliott, *An Introduction to Guided Waves and Microwave Circuits*. London, U.K.: Prentice-Hall, 1993.

[6] C. Seguinot, P. Kennis, J.-F. Legier, F. Huret, E. Paleczny, and L. Hayden, "Multimode TRL. A new concept in microwave measurements: Theory and experimental verification," *IEEE Trans. Microw. Theory Techn.*, vol. 46, no. 5, pp. 536–542, May 1998.

[7] V. Rizzoli, "Resonance measurement of even and odd mode propagation constants in coupled microstrips," in *Proc. IEEE-MTT-S Int. Microw. Symp.*, 1975, pp. 106–108.

[8] J. G. Richings and B. Easter, "Measured odd- and even-mode dispersion of coupled microstrip lines (short papers)," *IEEE Trans. Microw. Theory Techn.*, vol. 23, no. 10, pp. 826–828, Oct. 1975.

[9] T.-M. Winkel, L. Dutta, H. Grabinski, and E. Groteluschen, "Determination of the propagation constant of coupled lines on chips based on high frequency measurements," in *Proc. IEEE Multi-Chip Module Conf.*, 1996, pp. 99–104.

[10] A. Hernández-Escobar, E. Abdo-Sánchez, J. Esteban, T. M. Martín-Guerrero, and C. Camacho-Peñalosa, "Broadband determination of the even- and odd-mode propagation constants of coupled lines based on two-port measurements," *IEEE Trans. Microw. Theory Techn.*, vol. 68, no. 2, pp. 648–654, Feb. 2020.

[11] K. Kang, J. Brinkhoff, J. Shi, and F. Lin, "On-chip coupled transmission line modeling for millimeter-wave applications using four-port measurements," *IEEE Trans. Adv. Packag.*, vol. 33, no. 1, pp. 153–159, Feb. 2010.

[12] Y. Eo, W. Eisenstadt, and J. Shim, "S-parameter-measurement-based high-speed signal transient characterization of VLSI interconnects on SiO/sub 2/-Si substrate," *IEEE Trans. Adv. Packag.*, vol. 23, no. 3, pp. 470–479, Aug. 2000.

[13] D. Williams, "Multiconductor transmission line characterization," *IEEE Trans. Compon., Packag., Manuf. Technol.: Part B*, vol. 20, no. 2, pp. 129–132, May 1997.

[14] Y. Shlepnev, "Broadband material model identification with GMS-parameters," in *Proc. IEEE 24th Elect. Perform. Electron. Packag. Syst.*, 2015, pp. 155–158.

[15] K. Murakami, "Systematic mixed even- and odd-mode modeling of parallel tightly coupled transmission lines," in *Proc. 53rd IEEE Int. Midwest Symp. Circuits Syst.*, 2010, pp. 153–156.

[16] P. Gomez-Jimenez, P. Otero, and E. Marquez-Segura, "Analysis and design procedure of transmission-line transformers," *IEEE Trans. Microw. Theory Techn.*, vol. 56, no. 1, pp. 163–171, Jan. 2008.

[17] D. Bockelman, W. Eisenstadt, and R. Stengel, "Accuracy estimation of mixed-mode scattering parameter measurements," *IEEE Trans. Microw. Theory Techn.*, vol. 47, no. 1, pp. 102–105, Jan. 1999.

[18] C.-C. Huang and Y.-C. Chen, "Differential- and common-mode characterization of coupled interconnect transmission lines using four-port S-parameter measurements," in *Proc. 5th Int. Microsystems Packag. Assem. Circuits Technol. Conf.*, 2010, pp. 1–4.

[19] D. Williams and R. Marks, "Transmission line capacitance measurement," *IEEE Microw. Guided Wave Lett.*, vol. 1, no. 9, pp. 243–245, Sep. 1991.

[20] M. Wojnowski, V. Issakov, G. Sommer, and R. Weigel, "Multimode TRL calibration technique for characterization of differential devices," *IEEE Trans. Microw. Theory Techn.*, vol. 60, no. 7, pp. 2220–2247, Jul. 2012.

[21] L. Wan, Q. Li, Z. Wang, and J. Wu, "Improved multimode TRL calibration method for characterization of homogeneous differential discontinuities," *IEEE Trans. Instrum. Meas.*, vol. 64, no. 3, pp. 694–703, Mar. 2015.

[22] R. B. Marks, "A multiline method of network analyzer calibration," *IEEE Trans. Microw. Theory Techn.*, vol. 39, no. 7, pp. 1205–1215, Jul. 1991.

[23] M. Kirschning and R. H. Jansen, "Accurate wide-range design equations for the frequency-dependent characteristic of parallel coupled microstrip lines," *IEEE Trans. Microw. Theory Techn.*, vol. 32, no. 1, pp. 83–90, Jan. 1984.

[24] D. Bockelman and W. Eisenstadt, "Combined differential and common-mode scattering parameters: Theory and simulation," *IEEE Trans. Microw. Theory Techn.*, vol. 43, no. 7, pp. 1530–1539, Jul. 1995.

[25] A. Huynh, P. Hakansson, and S. Gong, "Mixed-mode S-parameter conversion for networks with coupled differential signals," in *Proc. Eur. Microw. Conf.*, 2007, pp. 238–241.

[26] W. R. Eisenstadt, B. Stengel, and B. M. Thompson, *Microwave Differential Circuit Design Using Mixed-Mode S-Parameters*. Norwood, MA, USA: Artech House, 2006.

[27] D. E. Bockelman and W. R. Eisenstadt, "Pure-mode network analyzer for on-wafer measurements of mixed-mode S-parameters of differential circuits," *IEEE Trans. Microw. Theory Techn.*, vol. 45, no. 7, pp. 1071–1077, Jul. 1997.

[28] B. Bianco and M. Parodi, "Measurement of the effective relative permittivities of microstrip," *Electron. Lett.*, vol. 3, no. 11 pp. 71–72, Feb. 1975.

[29] G. F. Engen and C. A. Hoer, "Thru-reflect-line: An improved technique for calibrating the dual six-port automatic network analyzer," *IEEE Trans. Microw. Theory Techn.*, vol. 27, no. 12, pp. 987–993, Dec. 1979.

[30] A. Jones, S. Lucyszyn, E. Márquez-Segura, N. Ridler, J. Skinner, and D. Stokes, "3-D printed primary standards for calibration of microwave network analysers," *Measurement*, vol. 158, 2020, Art. no. 107682. [Online]. Available: http://www.sciencedirect.com/science/article/pii/S0263224120302207

[31] B. Bianco, M. Parodi, S. Ridella, and F. Selvaggi, "Launcher and microstrip characterization," *IEEE Trans. Instrum. Meas.*, vol. IM-25, no. 4, pp. 320–323, Dec. 1976.

[32] R. B. Marks and D. F. Williams, "Characteristic impedance determination using propagation constant measurement," *IEEE Microw. Guided Wave Lett.*, vol. 1, no. 6, pp. 141–143, Jun. 1991.

[33] T. Jensen, V. Zhurbenko, V. Krozer, and P. Meincke, "Coupled transmission lines as impedance transformer," *IEEE Trans. Microw. Theory Techn.*, vol. 55, no. 12, pp. 2957–2965, Dec. 2007.

This article has been accepted for inclusion in a future issue of this journal. Content is final as presented, with the exception of pagination.

IEEE Journal of
Microwaves

[34] J. V. Heuven and T. Rozzi, "The invariance properties of a multivalue n-port in a linear embedding," *IEEE Trans. Circuit Theory*, vol. 19, no. 2, pp. 176–183, Mar. 1972.

[35] M. Pérez-Escribano and E. Márquez-Segura, "Random errors in broadband characterization of the propagation constant of transmission lines using multiple two-port measurements," *IEEE Access*, vol. 9, pp. 59038–59047, 2021.

[36] "Ansys HFSS software," 2021. [Online]. Available: https://www.ansys.com/products/electronics/ansys-hfss

[37] "RO4000 series high frequency circuit materials," 2021. [Online]. Available: https://rogerscorp.com/-/media/project/rogerscorp/documents/advanced-connectivity-solutions/english/data-sheets/ro4000-laminates-ro4003c-and-ro4350b-data-sheet.pdf

[38] A. Sabban and K. Gupta, "Characterization of radiation loss from microstrip discontinuities using a multiport network modeling approach," *IEEE Trans. Microw. Theory Techn.*, vol. 39, no. 4, pp. 705–712, Apr. 1991.

[39] X. Liu, C. Christopoulos, and D. W. P. Thomas, "Prediction of radiation losses and emission from a bent wire by a network model," *IEEE Trans. Electromagn. Compat.*, vol. 48, no. 3, pp. 476–484, Aug. 2006.

[40] D. Pozar, *Microwave Engineering*, 2nd ed. New York, NY, USA: Wiley, 1998.

[41] C. Schuster and W. Fichtner, "Parasitic modes on printed circuit boards and their effects on EMC and signal integrity," *IEEE Trans. Electromagn. Compat.*, vol. 43, no. 4, pp. 416–425, Nov. 2001.

[42] M. Steer, *Microwave and RF Design, Vol. 2: Transmission Lines* (Microwave and RF Design Series). Chapel Hill, NC, USA: Univ. North Carolina Press, 2019. [Online]. Available: https://books.google.es/books?id=J3avxwEACAAJ

[43] E. Hammerstad and O. Jensen, "Accurate models for microstrip computer-aided design," in *IEEE MTT-S Int. Microw. Symp. Dig.*, 1980, pp. 407–409.

MARIO PÉREZ-ESCRIBANO (Graduate Student Member, IEEE) was born in Alcalá la Real, Jaén, Spain, in December 1993. He received the B.S. degree in telecommunication engineering from the University of Málaga, Málaga, Spain, in 2015, the M.S. degree in telecommunication engineering from the University Carlos III de Madrid, Madrid, Spain, in 2017, and the Ph.D. degree from the Departamento de Ingeniería de Comunicaciones, Escuela Técnica Superior de Ingeniería deTelecomunicación, Universidad de Málaga, in 2022. In 2014, he joined the Departamento de Ingeniería de Comunicaciones, Escuela Técnica Superior de Ingeniería de Telecomunicación, Universidad de Málaga. In 2019, he did a research stay with the NASA Jet Propulsion Laboratory, USA. His research interests include analysis of structures made by additive manufacturing techniques, planar circuits, and dielectric resonator antennas. Mr. Pérez-Escribano was the recipient of the Spanish Ministry of Education, Culture, and Sports Scholarship for the term 2017–2022.

ENRIQUE MÁRQUEZ-SEGURA (Senior Member, IEEE) was born in Málaga, Spain, in April 1970. He received the Ingeniero de Telecomunicación and Doctor Ingeniero degrees from the Universidad de Málaga, Málaga, Spain, in 1993 and 1998, respectively. In 1994, he joined the Departamento de Ingeniería de Comunicaciones, Escuela Técnica Superior de Ingeniería de Telecomunicación, Universidad de Málaga, where he became an Associate Professor in 2001. His research interests include electromagnetic material characterization, additive manufacturing of electromagnetic devices, measurement techniques, RF, microwave, and millimeter-wave circuits design for communication and automotive applications. He was the recipient of the Spanish Ministry of Education and Science Scholarship, from 1994 to 1995. Since 2017, he has been a Visiting Researcher with the Department of Electrical and Electronic Engineering, Imperial College London, London, U.K. From 2020 to 2023, he was the Chair of Spain joint Chapter of IEEE Antennas and Propagation and Microwave Theory and Technologies Societies.